



N^6 -Methyladenosine Modification in a Long Noncoding RNA Hairpin Predisposes Its Conformation to Protein Binding

Katherine I. Zhou¹, Marc Parisien², Qing Dai³, Nian Liu³, Luda Diatchenko², Joseph R. Sachleben⁴ and Tao Pan^{5,6}

¹ - Medical Scientist Training Program, The University of Chicago, Chicago, IL 60637, USA

² - The Alan Edwards Centre for Research on Pain, McGill University, Montréal, QC, Canada H3A 0G4

³ - Department of Chemistry, The University of Chicago, Chicago, IL 60637, USA

⁴ - Biomolecular NMR Core Facility, Biological Sciences Division, The University of Chicago, Chicago, IL 60637, USA

⁵ - Department of Biochemistry and Molecular Biology, The University of Chicago, Chicago, IL 60637, USA

⁶ - Institute of Biophysical Dynamics, The University of Chicago, Chicago, IL 60637, USA

Correspondence to Tao Pan: Department of Biochemistry and Molecular Biology, The University of Chicago, Chicago, IL 60637, USA. taopan@uchicago.edu

<http://dx.doi.org/10.1016/j.jmb.2015.08.021>

Edited by A. Pyle

Abstract

N^6 -Methyladenosine (m^6A) is a reversible and abundant internal modification of messenger RNA (mRNA) and long noncoding RNA (lncRNA) with roles in RNA processing, transport, and stability. Although m^6A does not preclude Watson–Crick base pairing, the N^6 -methyl group alters the stability of RNA secondary structure. Since changes in RNA structure can affect diverse cellular processes, the influence of m^6A on mRNA and lncRNA structure has the potential to be an important mechanism for m^6A function in the cell. Indeed, an m^6A site in the lncRNA metastasis associated lung adenocarcinoma transcript 1 (MALAT1) was recently shown to induce a local change in structure that increases the accessibility of a U_5 -tract for recognition and binding by heterogeneous nuclear ribonucleoprotein C (HNRNPC). This m^6A -dependent regulation of protein binding through a change in RNA structure, termed “ m^6A -switch”, affects transcriptome-wide mRNA abundance and alternative splicing. To further characterize this first example of an m^6A -switch in a cellular RNA, we used nuclear magnetic resonance and Förster resonance energy transfer to demonstrate the effect of m^6A on a 32-nucleotide RNA hairpin derived from the m^6A -switch in MALAT1. The observed imino proton nuclear magnetic resonance resonances and Förster resonance energy transfer efficiencies suggest that m^6A selectively destabilizes the portion of the hairpin stem where the U_5 -tract is located, increasing the solvent accessibility of the neighboring bases while maintaining the overall hairpin structure. The m^6A -modified hairpin has a predisposed conformation that resembles the hairpin conformation in the RNA–HNRNPC complex more closely than the unmodified hairpin. The m^6A -induced structural changes in the MALAT1 hairpin can serve as a model for a large family of m^6A -switches that mediate the influence of m^6A on cellular processes.

© 2015 Elsevier Ltd. All rights reserved.

Introduction

RNA modifications are important modulators of the structure and function of cellular RNAs. While the numerous modifications found in transfer RNA and ribosomal RNA have been extensively studied, much less is known about the function of the comparatively sparse modifications found in messenger RNA (mRNA) and long noncoding RNA (lncRNA). Three

types of internal mRNA and lncRNA modifications have been identified in higher eukaryotes so far [1–6]. Of these, N^6 -methyladenosine (m^6A) is the most abundant, with more than 12,000 m^6A sites in over 7000 genes in the human transcriptome [2–4,7]. A reversible modification, m^6A occurs within RRm⁶ACH motifs (R = A/G, H = A/C/U), with a high density of m^6A sites near stop codons and in long internal exons [3,4]. The m^6A methyltransferase complex is

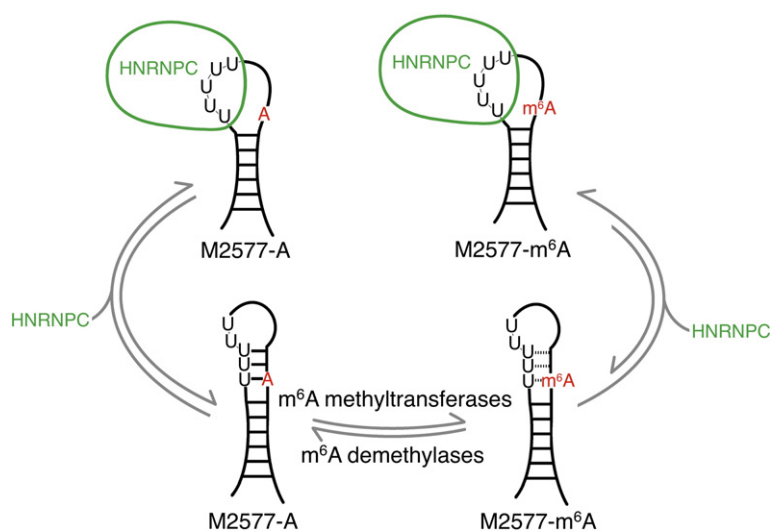


Fig. 1. The m^6A -switch model. The human lncRNA MALAT1 is reversibly methylated at position A2577. The protein HNRNPC binds to the U₅-tract in this hairpin from MALAT1, with an ~8-fold higher affinity for the methylated hairpin. One of the Us in the HNRNPC binding site pairs with the methylation site A2577. The presence of m^6A weakens the base pair and increases the accessibility of the U-tract for protein binding.

composed of the proteins methyltransferase-like METTL3 and METTL14 and the Wilms tumor 1 associated protein WTAP [8,9]. Two known demethylases, fat mass and obesity associated protein and AlkB family member 5, are responsible for removing m^6A modifications [10,11]. Perturbations to these enzymes lead to altered m^6A levels and affect diverse processes including metabolism, spermatogenesis, the circadian clock, and stem cell differentiation [10–15].

m^6A modification has functional roles in RNA splicing, nuclear export, and decay [16–19]. One mechanism for these functions is the recognition of m^6A by reader proteins. Several m^6A readers identified to date contain a YT521-B homology (YTH) domain that specifically binds m^6A in an aromatic cage [20–22]. Recently, the protein heterogeneous nuclear ribonucleoprotein C (HNRNPC) was identified as an m^6A reader that lacks a YTH domain. Instead, the recognition of m^6A by HNRNPC depends on an m^6A -induced change in RNA structure [19]. While m^6A is capable of Watson–Crick base pairing, thermal denaturation studies with model RNA duplexes have demonstrated that m^6A in a duplex is destabilizing by 0.5–1.7 kcal/mol [23,24]. To allow hydrogen bonding at the Watson–Crick face, the N^6 -methyl is in the *anti* position relative to the N1 across the C6–N6 bond [23]. The destabilization of the duplex by m^6A methylation is likely due to the steric clash between N7 and the *anti* N^6 -methyl in base-paired m^6A [23]. Since HNRNPC binds single-stranded U-tract motifs, methylation of an adenosine in a hairpin stem can destabilize the duplex to expose an HNRNPC binding site [25,26]. This “ m^6A -switch” mechanism was found to be the basis by which HNRNPC recognizes m^6A modification at a site in the human lncRNA metastasis associated lung adenocarcino-

ma transcript 1 (MALAT1). Further examination of HNRNPC-bound RNAs revealed 2798 high-confidence m^6A -switches in which HNRNPC is thought to use a similar mechanism of indirect m^6A recognition [19]. Likewise, other mRNA/lncRNA binding proteins could recognize m^6A indirectly via m^6A -induced changes in the availability of their structured or single-stranded binding sites. m^6A -switch-like RNAs could thus represent a widespread mechanism of m^6A function in the cell.

Dynamic RNA structures have extensive roles in the function of structural and regulatory lncRNAs and in the regulation of mRNA transcription, splicing, translation, and stability [27]. Thus, the effect of m^6A on lncRNA and mRNA structure has the potential to influence many cellular processes. *In vitro* studies with model m^6A duplexes have demonstrated that m^6A can either stabilize or destabilize RNA secondary structures depending on its position within or at the end of a duplex [23]. Further evidence suggests that m^6A influences RNA structure *in vivo*. Parallel analysis of RNA structure showed that RRACH motifs containing m^6A have a different RNA structural profile than RRACH motifs lacking m^6A modification [23]. Moreover, structural probing in an *in vivo* click-selective 2'-hydroxyl acylation and profiling experiment revealed a METTL3-dependent enhancement in reactivity at m^6A sites [28]. The widespread influence of m^6A on RNA secondary structure in cells could potentially have important consequences for the processing, function, and fate of mRNAs and lncRNAs.

The discovery that an m^6A -switch regulates HNRNPC binding revealed that m^6A -induced changes in mRNA and lncRNA structure have functional effects *in vivo*. In this study, we further characterized the m^6A -induced structural changes in a 32-nucleotide hairpin derived from the

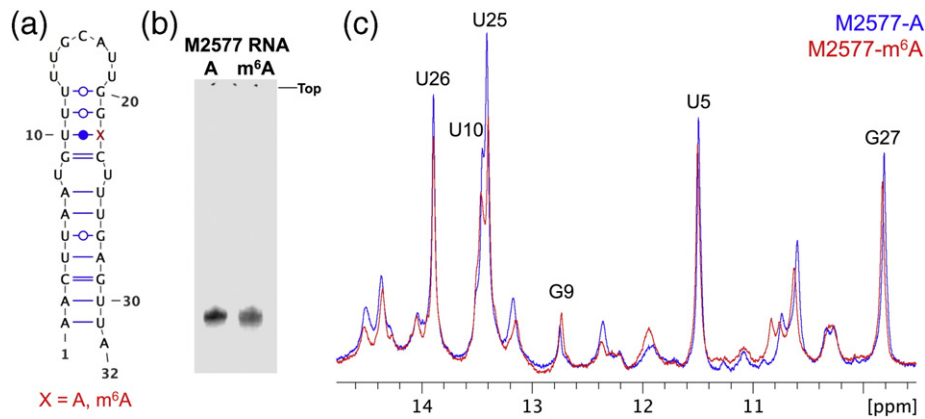


Fig. 2. 1D NMR spectra show that the overall structure of the hairpin is maintained. (a) Secondary structure of the 32-nucleotide M2577-A oligo from nucleotides 2556–2587 of MALAT1. The m⁶A modification site (A22 in the oligo or A2577 in MALAT1) is denoted with a red “X”. The figure was made using visualization applet for RNA (VARNA) [30]. (b) Native PAGE (15%) of the unmodified (M2577-A) and methylated (M2577-m⁶A) hairpins in 25 mM Tris–acetate (pH 7.4) and 2.5 mM magnesium acetate. (c) Superimposed imino regions of the 1D ¹H NMR spectra of M2577-A (blue) and M2577-m⁶A (red). Watergate solvent suppression 1D ¹H NMR spectra were measured under the conditions 1.12 mM RNA, 10 mM Na₂HPO₄ (pH 7.4), 2.5 mM MgCl₂, and 90% H₂O/10% D₂O (v/v), at 20 °C.

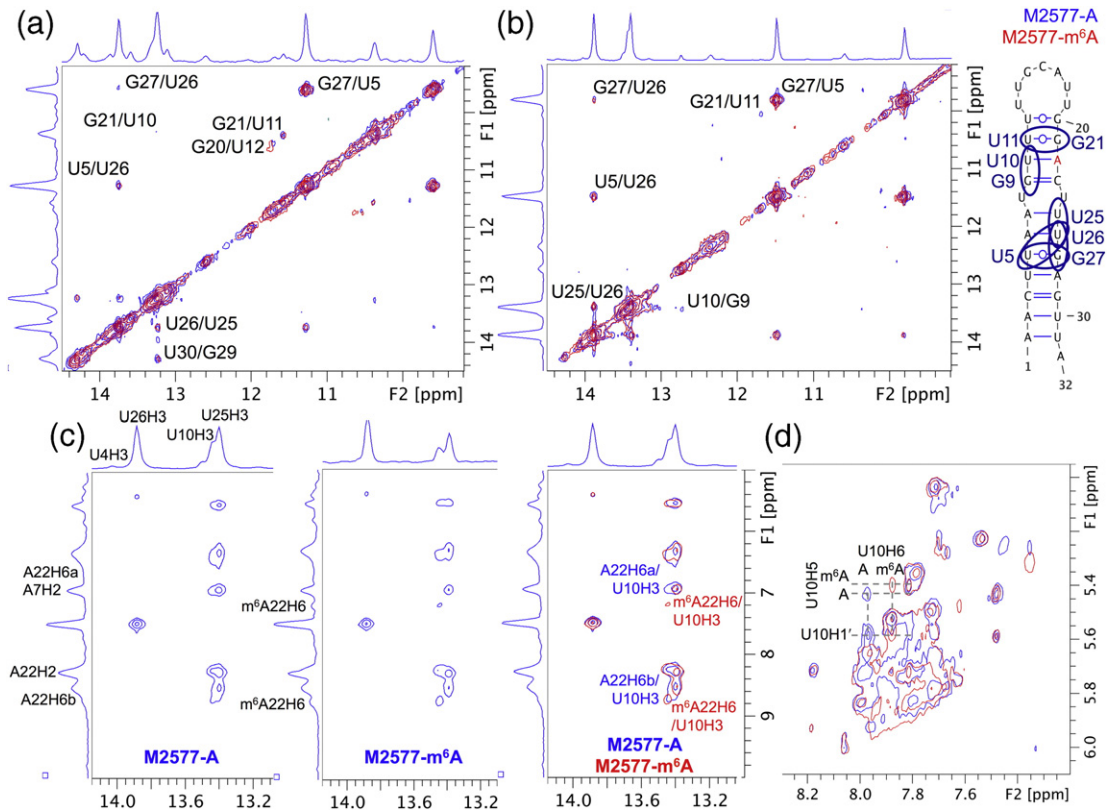


Fig. 3. 2D NOESY spectra show that the upper stem is more dynamic in the methylated than in the unmodified M2577 hairpin. (a) Superimposed imino regions of the 2D ¹H NOESY NMR spectra of M2577-A (blue) and M2577-m⁶A (red) in 10% D₂O. The spectra of 0.47 mM RNA were measured at 4 °C with a 100-ms mixing time. (b) Superimposed imino regions of the 2D ¹H NOESY NMR spectra of M2577-A and M2577-m⁶A in 10% D₂O. The spectra of 1.12 mM RNA were measured at 20 °C with a 100-ms mixing time. (c) Separate and superimposed amino–imino regions of the 2D ¹H NOESY NMR spectra of M2577-A and M2577-m⁶A in 10% D₂O at 20 °C. (d) Superimposed H6/H8–H1' regions of the 2D ¹H NOESY NMR spectra of M2577-A and M2577-m⁶A in 100% D₂O. The spectra of 0.78 mM RNA were measured at 20 °C with a 100-ms mixing time.

Table 1. Imino–imino NOE intensity in 10% D₂O at 20 °C

Imino–imino pair	NOE intensity for M2577-A	NOE intensity for M2577-m ⁶ A
G27H1–U5H3	1.00 ± 0.00	1.00 ± 0.00
U5H3–U26H3	0.20 ± 0.02	0.17 ± 0.03
U25H3–U26H3	0.16 ± 0.03	0.18 ± 0.01
G27H1–U26H3	0.06 ± 0.01	0.06 ± 0.00
G21H1–U11H3	0.05 ± 0.02	0.00 ± 0.01
G9H1–U10H3	0.04 ± 0.01	0.01 ± 0.00

m⁶A-switch in the human lncRNA MALAT1. Nuclear magnetic resonance (NMR) revealed that, while the methylated hairpin maintains its overall structure, m⁶A affects the distances between protons in the hairpin region where m⁶A is located. Förster resonance energy transfer (FRET) studies further demonstrated that m⁶A alters the conformation of the MALAT1 hairpin to become more similar to the HNRNPC-bound hairpin, whereas HNRNPC binding induces similar conformations of both methylated and unmethylated hairpins. Comparing A and m⁶A hairpins shows that m⁶A modification predisposes the RNA conformation to resemble more closely its conformation in the RNA–HNRNPC complex.

Results

In previous studies, HNRNPC was found to preferentially bind an m⁶A-modified hairpin composed of nucleotides 2556–2587 of the lncRNA MALAT1, with an ~8-fold higher affinity for the methylated hairpin [19]. Since HNRNPC is known to recognize single-stranded U-tracts of at least 5 Us in length, it was hypothesized that methylation of A2577 destabilizes the hairpin stem, exposing the single-stranded U-tract for HNRNPC binding (Fig. 1) [19,25,26]. Structural probing with RNase V1 and S1 nuclease was consistent with this m⁶A-switch model, showing decreased stacking and increased single strandedness in the region of the hairpin stem surrounding A2577 upon m⁶A modification [19,29]. However, it was not known how extensive the global structural and dynamic differences are between the unmodified and m⁶A-modified hairpins and how m⁶A modification enhances HNRNPC binding to the MALAT1 hairpin. We address these questions here using NMR and FRET methods.

NMR shows that methylation of the MALAT1 hairpin changes the conformation of a portion of the hairpin stem

To examine the differences between the methylated and unmethylated MALAT1 hairpin in solution, we collected 1D ¹H NMR spectra of both hairpins at 20 °C in 10% D₂O (Fig. 2a–c). Native gel electrophoresis demonstrated that the hairpins migrate as a

single major species with the same mobility regardless of methylation status (Fig. 2b). The 1D spectra of the two hairpins are largely similar, suggesting that the overall structure of the hairpin is maintained. In particular, the 9.5- to 14.8-ppm regions show that the chemical shifts of the imino protons H1 and H3 of G and U, respectively, are largely unaffected by methylation of the hairpin (Fig. 2c).

We performed 2D nuclear Overhauser enhancement spectroscopy (NOESY) experiments of the methylated and unmethylated MALAT1 hairpins at 4 °C and 20 °C in 10% D₂O to assign the imino protons and to detect differences in inter-proton distances (Fig. 3a and b and Table 1). Sequential nuclear Overhauser enhancements (NOEs) between imino protons of neighboring guanosines and uridines were used for imino proton assignments. Many of the same imino–imino NOEs were present in both methylated and unmethylated hairpins, suggesting that these base–base interactions are maintained and the overall structure of the hairpin does not change upon m⁶A modification. However, two imino–imino NOEs were observed at 20 °C in the unmethylated hairpin, but not in the methylated hairpin: an NOE between the imino protons of U11 and G21 and an NOE between the imino protons of G9 and U10. Both NOEs involve bases within the U-tract that consists of the binding site for HNRNPC protein. The loss of these NOEs suggests a change in conformation in the upper part of the MALAT1 hairpin stem. Since NOEs are an indicator of through-space distance, where NOE signal falls rapidly with distance r as $1/r^6$, the loss of the NOE between U11 and G21 imino protons in particular is consistent with the model that this portion of the stem is less stably base paired in the methylated hairpin.

In addition, the methylated hairpin exhibited several changes in the amino–imino region of the NOESY spectrum (Fig. 3c). The most pronounced changes were found in NOEs between amino region protons and the imino proton of U10. These amino region resonances likely correspond to protons from the A/m⁶A22 that base pairs with U10. Similar to previous NMR studies with model m⁶A duplexes, we observed NOEs of the m⁶A22 H2 and H6 with the imino proton of the base-paired U10 [23]. Two NOEs were observed between the m⁶A22 H6 and the imino proton of U10, suggesting slow exchange between the *anti* and *syn* conformations of the N⁶-methyl group. The NOEs of the U10 imino proton with the m⁶A22 H6 proton were stronger than those with the A22 H6a and H6b protons of the unmethylated hairpin, likely due to slower rotation of the N⁶-methylamino group, as has been previously proposed [23]. The NOE between the U10 imino and the A/m⁶A22 H2 was equally intense in the methylated and unmethylated hairpins, suggesting that the hydrogen bond between the U10 imino

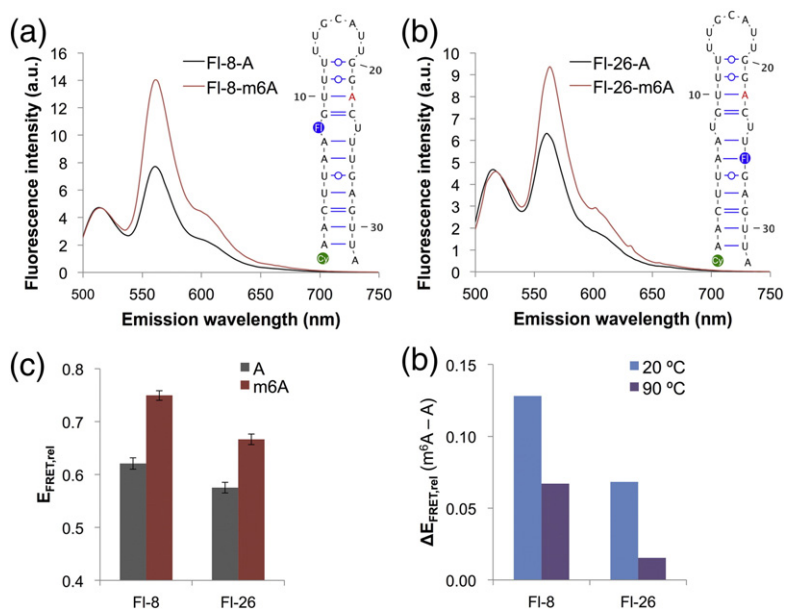


Fig. 4. FRET shows that the methylated and unmethylated MALAT1 hairpins have different conformations. (a) Fluorescence emission spectra of the FRET constructs FI-8-A and FI-8-m⁶A upon excitation at 490 nm. Cy3 (green) is conjugated to the 5' phosphate, and fluorescein-dT (FI) is incorporated at the indicated position (blue) in each oligo. Spectra were measured under the conditions 500 nM RNA, 10 mM Tris (pH 7.5), 100 mM KCl, and 2.5 mM MgCl₂ at ambient temperature. Each spectrum is the average of 2–3 measurements. (b) Fluorescence emission spectra of FI-26-A and FI-26-m⁶A upon excitation at 490 nm. (c) Relative FRET efficiencies ($E_{\text{FRET,rel}}$) of M2577-A and M2577-m⁶A, calculated as $I_{563}/(I_{563} + I_{518})$, where I_x is the fluorescence emission intensity at x nm. FRET efficiencies are the mean of 6–8 measurements. Error bars represent ± 1 standard deviation. (d) Difference in the relative FRET efficiencies of M2577-A and M2577-m⁶A at ambient temperature (~ 20 °C) or at 90 °C.

proton and m⁶A22 N1 is retained. Given that the single m⁶A22 H6 proton shows two NOEs with the U10 imino proton, the m⁶A–U base pair could be either singly or doubly hydrogen bonded within the hairpin depending on the *syn* or *anti* conformation of the N⁶-methyl group in m⁶A. Previous studies with model m⁶A duplexes found only one NOE between the m⁶A H6 and the U imino [23]. This discrepancy is consistent with previous observations that the effect of m⁶A on stability is strongly context dependent [23,24]. The m⁶A–U was two G–C pairs from the end of the model m⁶A duplex used for NMR studies by Roost *et al.* [23], whereas in the MALAT1 hairpin, the m⁶A–U is two G–U pairs from the loop, which could afford more flexibility for the N⁶-methylamino group to rotate.

We further collected 2D NOESY spectra of the methylated and unmethylated MALAT1 hairpins at 20 °C in 100% D₂O (Fig. 3d). The resonances were broad and overlapping, such that the intra- and inter-nucleotide H6/H8–H1' NOEs along the duplex could not be traced unambiguously. Nonetheless, a comparison between the NOESY spectra of the methylated and unmethylated hairpins showed that the H6/H8–H1' regions were mostly similar, but with several distinct shifts in resonances. These shifted resonances most likely correspond to protons of the m⁶A22–U10 base pair or of nearby nucleotides.

Similar shifts in resonances have been observed in studies with model m⁶A duplexes [23].

FRET shows that the methylated and unmethylated hairpins have different conformations

To further probe the influence of m⁶A on the conformation of the MALAT1 hairpin in solution, we designed two pairs of unmethylated and methylated MALAT1 hairpins modified with a 5' indocarbocyanine-3 (Cy3) fluorophore and an internal fluorescein fluorophore in the hairpin stem (Fig. 4a and b). The constructs were named based on the position of the fluorescein fluorophore: the unmethylated and methylated hairpins FI-8-A and FI-8-m⁶A contain fluorescein-dT at nucleotide position 8, while the unmethylated and methylated hairpins FI-26-A and FI-26-m⁶A contain fluorescein-dT at nucleotide position 26.

We observed that m⁶A modification resulted in a significant increase in FRET efficiency at ambient temperature (Fig. 4a–c). In contrast, the methylated and unmethylated hairpins had similar FRET efficiencies when denatured at 90 °C (Fig. 4d). Based on these results, we suggest that m⁶A increases the FRET efficiency by altering the conformation of the MALAT1 hairpin, whereas m⁶A does not alter the conformation

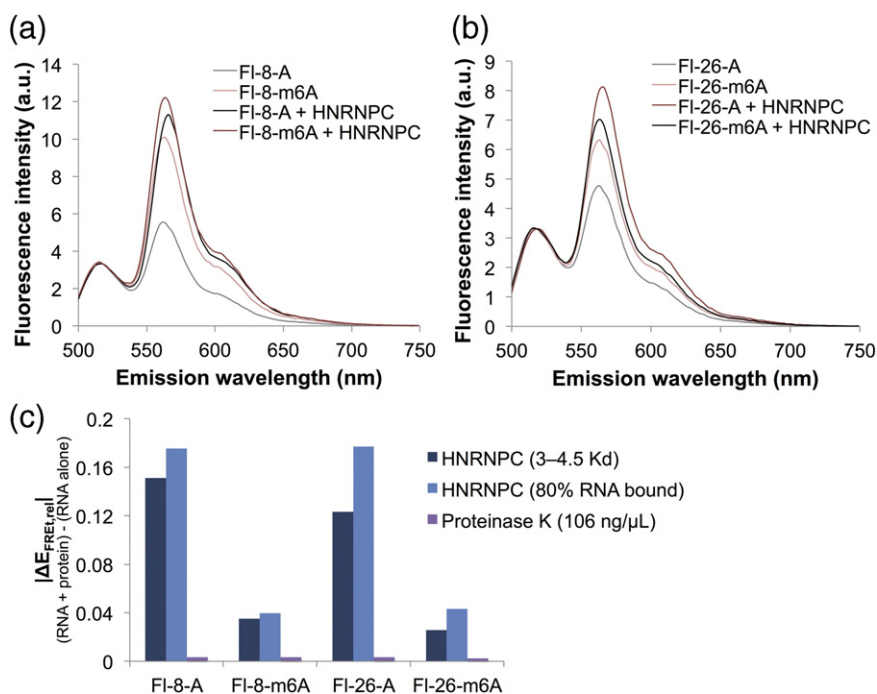


Fig. 5. FRET of RNPs containing the M2577-A and M2577- m^6A hairpins. The RNPs show similar FRET, suggesting that the conformation of the RNA in the RNP is the same regardless of the presence of m^6A . In addition, the methylated hairpins exhibit a smaller change in FRET upon HNRNPC binding. (a) Fluorescence emission spectra of 500 nM FI-8-A and FI-8- m^6A with or without addition of HNRNPC at a concentration of $3\text{--}4.5 \times K_d$ ($K_d = 722$ nM for M2577-A; $K_d = 93$ nM for M2577- m^6A) [19]. Spectra were measured under the conditions 500 nM RNA, 10 mM Tris (pH 7.5), 100 mM KCl, and 2.5 mM MgCl_2 at ambient temperature at excitation wavelength 490 nm. (b) Fluorescence emission spectra of 500 nM FI-26-A and FI-26- m^6A with or without addition of HNRNPC at a concentration of $3\text{--}4.5 \times K_d$. (c) Change in the relative FRET efficiency ($\Delta E_{\text{FRET,rel}}$) of each hairpin (500 nM) upon addition of $3\text{--}4.5 \times K_d$ HNRNPC (2.17 μM HNRNPC for M2577-A; 410 nM HNRNPC for M2577- m^6A), HNRNPC such that $[\text{RNP}]/[\text{RNA}]_{\text{total}} = 80\%$ (3.29 μM HNRNPC for M2577-A; 770 nM HNRNPC for M2577- m^6A), or 106 ng/ μL proteinase K (equivalent to weight/volume concentration of 3.25 μM HNRNPC).

of the unfolded oligo. Changes in FRET efficiency could be due to changes in the distance between donor and acceptor fluorophores or to changes in the relative orientation of the fluorophores. Since the fluorescein donor fluorophore was in the stem of the MALAT1 hairpin, increased flexibility of the hairpin stem upon m^6A modification could alter the position or orientation of the fluorescein fluorophore to increase the efficiency of energy transfer to Cy3 at the 5' end of the hairpin. This interpretation of the observed FRET efficiencies is consistent with the m^6A -switch model for the MALAT1 hairpin in which m^6A modification increases the flexibility of the hairpin stem and exposes single-stranded RNA for protein binding.

FRET shows that the conformation of the methylated hairpin is more similar to the HNRNPC-bound RNA conformation

The abovementioned results demonstrate that m^6A modification of the MALAT1 hairpin changes the conformation of the RNA alone. To evaluate the influence of m^6A modification on the conformation of

the HNRNPC-bound hairpin, we added HNRNPC protein to the MALAT1 hairpin constructs and measured the resulting FRET spectra. The FRET efficiencies of the methylated and unmethylated MALAT1 hairpins became more similar upon addition of HNRNPC (Fig. 5a and b), whereas the FRET efficiencies did not change upon addition of proteinase K as a control protein (Fig. 5c). Thus, although m^6A modification alters the conformation of the MALAT1 hairpin alone, in the ribonucleoprotein (RNP) complex, the RNA has the same conformation regardless of modification status. We suggest that the difference in the affinity of HNRNPC for the methylated and unmethylated hairpins is the result of a difference in the conformation of the unbound RNA hairpins, whereas the RNPs have the same conformation and energetics regardless of RNA methylation. The 8-fold difference in the K_d for HNRNPC binding can be accounted for by a destabilization (~ 1.2 kcal/mol) of the hairpin duplex by m^6A to expose the U-tract for HNRNPC binding, consistent with the previously observed destabilizing effect (0.5–1.7 kcal/mol) of m^6A on model RNA duplexes

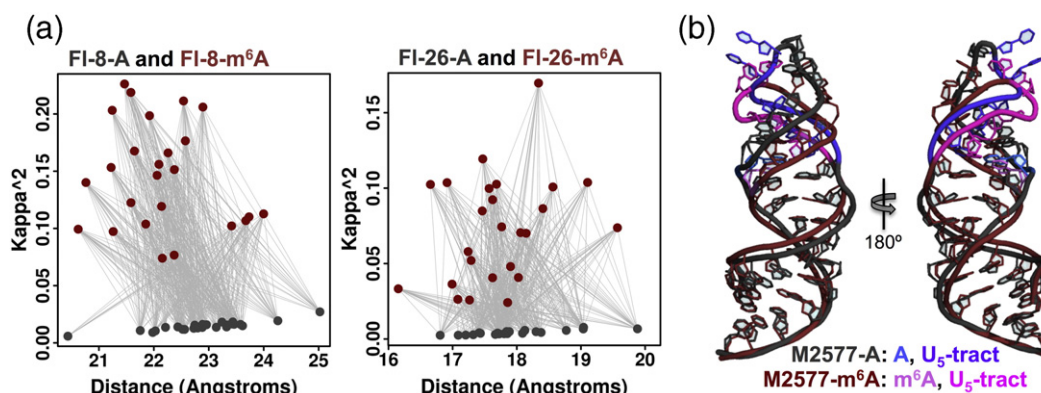


Fig. 6. Structural models for M2577-A and M2577-m⁶A based on FRET and NMR data. (a) Plot of 25 selected structures for M2577-A (gray) and M2577-m⁶A (dark red), in terms of κ^2 and distance between fluorophores for FI-8-A/m⁶A and FI-26-A/m⁶A. The structures were selected from an initial set of 9999 tertiary structures for the M2577 hairpin [31] (c) Structural models of M2577-A (gray) and M2577-m⁶A (dark red), computed as the centroid of the 25 selected structures. The m⁶A modification site and the U₅-tract are highlighted in shades of blue for the unmethylated MALAT1 hairpin and in magenta for the methylated hairpin.

[23]. The change in the stability of the RNA hairpin explains how formation of an RNP with the methylated hairpin is more thermodynamically favorable than formation of an RNP with the unmethylated hairpin, even though the methylated and unmethylated RNPs are similar in conformation and energy.

For both sets of constructs, the change in FRET efficiency upon protein binding was more drastic for the unmethylated hairpin than for the methylated hairpin (Fig. 5c), suggesting that the conformation of the methylated hairpin is more similar to that of the HNRNPC-bound hairpin. Since the conformations of the free and bound m⁶A-modified hairpin are similar, the conformational change in the conversion of the free form into the bound form might require less energy than the conversion of the unmodified hairpin from the free conformation to the bound conformation. In this manner, m⁶A modification seems to set up the hairpin for HNRNPC binding by inducing a conformation more similar to the protein-bound form.

Structural modeling shows how m⁶A can alter the conformation of the MALAT1 hairpin

Using the RNA tertiary structure prediction program MC-Sym [31], we generated 9999 models for the MALAT1 hairpin and selected models corresponding to the methylated and unmethylated hairpins based on four simultaneous criteria: (1) best fit to the FRET data, (2) best fit to the 2D NOESY data collected with 100 ms mixing time in 10% D₂O, (3) best P-Scores, and (4) maximization of relative FRET yields. While MC-Sym can use NMR data to guide model generation, FRET data involve pairs of models; thus, they are not amenable to interpretation during model generation. Instead of generating models based on the experimental data, we first generated a large pool of models then chose

those that satisfy all the data. True conformational sampling would require the use of molecular dynamics simulations, but due to very slow RNA dynamics, this approach is not attempted here.

The selected models were narrowed down to 25 models corresponding to the unmethylated hairpin and 25 models corresponding to the methylated hairpin. The parameters used to calculate the theoretical FRET efficiencies (the orientation parameter κ^2 and the distance between fluorophores) are plotted in Fig. 6a. While the distribution of distances is similar for both the “A” and “m⁶A” sets, the models corresponding to the methylated hairpin (m⁶A set) show more variation in the orientation parameter κ^2 . Since the position of the Cy3 fluorophore was kept invariant in all 9999 models, κ^2 depends primarily on the position and orientation of the fluorescein fluorophore in the hairpin stem. The observation that the m⁶A set shows more variation in κ^2 implies that a wider range of different fluorescein fluorophore orientations is consistent with the FRET and NMR data, raising the possibility that the bases in the stem of the methylated hairpin have greater dynamic flexibility or can adopt multiple distinct conformations.

The centroid of the 25 models was used to generate a single model each for methylated and unmethylated MALAT1 hairpins (Fig. 6b). The superimposed model structures reveal an m⁶A-methylation-dependent change in the conformation of the upper stem and loop of the MALAT1 hairpin, including the backbone and nucleobases of the U-tract bound by HNRNPC. Thus, m⁶A methylation of the hairpin induces a conformational change that propagates through the hairpin structure sufficiently to influence the structure of the HNRNPC binding site, which supports the model that the effect of m⁶A on the hairpin structure indirectly causes a change in the HNRNPC binding affinity.

Discussion

In this study, we used biophysical methods and modeling to examine the effect of m⁶A modification on the MALAT1 hairpin. Our NMR and FRET results demonstrate that the general structure of the MALAT1 hairpin is maintained, but the nucleobases of the hairpin stem are more flexible and solvent accessible upon m⁶A modification. These results support the m⁶A-switch model in which m⁶A regulates protein binding through its influence on RNA structure [19].

While previous studies examined the influence of m⁶A on the structure and stability of model RNA duplexes, no past studies used NMR to investigate a physiological m⁶A-modified RNA [23,24]. The study of nucleic acids by NMR is already challenging due to low proton density and high spectral overlap [32,33]. The terminal loop, internal loop, and noncanonical G–U pairs of the MALAT1 hairpin further complicate the detection and assignment of imino protons by reducing the number of detectable protons, interrupting the continuity of the stem, and introducing ambiguity in the assignment of imino–imino NOEs. The possibility of dynamic changes in structure, base pairing, and oligomerization state introduces additional difficulties in the study of a naturally occurring RNA hairpin. In the future, structural studies of physiological m⁶A-modified RNA might take advantage of selective labeling with ¹⁵N or ¹³C isotopes. Such methods would enable direct observation of hydrogen bonding, unambiguous identification of noncanonical base–base interactions, and better resolution of local changes in conformation [32,33].

The FRET constructs used in this study showed that m⁶A modification influences the observed FRET efficiency, likely due to an m⁶A-induced change in the conformation of the MALAT1 hairpin. However, ensemble FRET studies cannot distinguish a homogeneous population adopting a single conformation from a heterogeneous population with multiple subpopulations or with dynamically changing conformations [34]. It is possible that the m⁶A-modified hairpins not only have a different average structure but also are more dynamic or adopt a more heterogeneous set of different conformations. It would be very interesting to study our constructs using single-molecule FRET in order to better understand how m⁶A influences the conformational dynamics of the MALAT1 hairpin. Single-molecule FRET studies are well suited to studying dynamic systems and have provided insight into processes such as RNA folding and RNP formation [35]. In addition to clarifying the structure and dynamics of the MALAT1 hairpin, single-molecule FRET could further elucidate how m⁶A affects hairpin folding and protein binding.

The MALAT1 hairpin is the first identified example of an m⁶A-switch, but the changes induced by m⁶A

modification of the MALAT1 hairpin are likely generalizable to a much larger family of m⁶A-regulated RNA structures. Over 2000 high-confidence m⁶A-switches have been identified at HNRNPC binding sites [19]. In addition, the m⁶A-switch mechanism has the potential to regulate the binding of other RNA binding proteins through altered accessibility of their single-stranded RNA binding motifs or through changes in their cognate RNA structures. Thus far, the only m⁶A reader proteins known to directly bind m⁶A belong to the YTH family of proteins [18]. While other direct m⁶A binders might yet be discovered, the m⁶A-switch mechanism expands the pool of candidate m⁶A readers to a much wider array of RNA binding proteins. Indirect m⁶A readers might be pervasive but difficult to discover because, in many cases, only a subset of their targets might be regulated by m⁶A modification. For example, m⁶A-switches seem to regulate ~8% or ~40,000 of all known HNRNPC binding sites [19]. Moving forward, it will be important to investigate other indirect m⁶A readers and the mechanisms by which m⁶A alters RNA structure to influence protein binding.

As the most abundant post-transcriptional modification in eukaryotic mRNA and lncRNA, m⁶A could have pervasive regulatory roles in the regulation of mRNA transcription, splicing, and translation and in influencing the structure and function of lncRNAs. In addition, m⁶A modification might influence RNA structures in other classes of noncoding RNA. For example, m⁶A methylation of primary microRNAs has recently been shown to be crucial for recognition by the microprocessor complex, though it is unclear in this case whether m⁶A functions by influencing RNA structure or through direct recognition [36,37]. While m⁶A modification likely regulates many m⁶A-switches using the same mechanism as in the MALAT1 hairpin, m⁶A could potentially use other mechanisms to regulate RNA structures such as disrupting a tertiary hydrogen bond [7]. Even in an RNA stem–loop, the influence of m⁶A on RNA structure is dependent on context, as m⁶A can either stabilize or destabilize depending on its position. It will be important to investigate the diverse and context-dependent effects of m⁶A on RNA structure and dynamics and how these are linked to the functions of m⁶A in the cell. As the first example of an m⁶A-induced structural change in a cellular RNA, the MALAT1 m⁶A-switch is an initial model for a potentially much more general mechanism by which m⁶A achieves its functions in the cell.

Materials and methods

RNA synthesis and purification

RNA oligos containing two fluorophore modifications in each sequence were synthesized by Expedite DNA Synthesizer on a 1- μ mol scale. Cy3 phosphoramidite

and fluorescein-dT phosphoramidite were purchased from Glen Research. m⁶A phosphoramidite was prepared by following our reported procedure [38]. All the other phosphoramidites and beads were purchased from ChemGenes. After oligo synthesis, the RNA oligos were first deprotected by treatment with 30% ammonium hydroxide and ethanol (3:1, v/v) at 55 °C for 4 h. Once cooled to ambient temperature, the supernatant was dried in a SpeedVac and the resulting pellets were further deprotected by treatment with a mixture of dimethyl sulfoxide (100 µL) and hydrogen fluoride triethylamine (125 µL) at 65 °C for 2.5 h. After cooling to ambient temperature, 22.5 µL sodium acetate (3 M) and *n*-butanol (1 mL) were added, and the mixture was vortexed and precipitated at -80 °C for 1 h. After centrifugation, the supernatant was removed, and the pellets were washed with 70% ethanol and purified on a gel containing 8% acrylamide:bisacrylamide (29:1), 7 M urea, 89 mM Tris-borate (pH 8.3), and 2 mM Na₂EDTA (ethylenediamine-tetraacetic acid). RNA was excised from the gel by UV shadowing and eluted in 50 mM potassium acetate and 200 mM KCl (pH 7.5) by the crush-and-soak method. Eluted RNA was precipitated in ethanol then resuspended and stored in H₂O at -20 °C.

RNA oligos M2577-A and M2577-m⁶A were synthesized, deprotected, and purified in a similar way except that we used a MerMade synthesizer on a 5-µmol scale.

HNRNPC protein expression and purification

Rosetta BL21 *Escherichia coli* were transformed with a pGEX-6P-1 plasmid containing the full-length HNRNPC1 coding sequence inserted between the BamHI and XhoI restriction sites. The transformed bacteria were grown to saturation at 37 °C, 200 rpm in Luria-Bertani Lennox media with 100 µg/mL ampicillin and 50 µg/mL chloramphenicol then diluted 1:100, grown in the same culture media to an absorbance of ~0.6 at 600 nm, and induced with 2.5 mM isopropyl β-D-1-thiogalactoside. The bacteria were grown an additional 5 h at 37 °C and 200 rpm then harvested and sonicated at 4 °C. GST (glutathione S-transferase)-HNRNPC1 fusion protein was isolated from the soluble lysate using GST-Bind resin (Novagen) and then cleaved by GST-tagged PreScission Protease for 16 h at 4 °C. The purified full-length HNRNPC1 protein was stored in 10 mM Tris (pH 7.5), 100 mM KCl, 2.5 mM MgCl₂, and 30% glycerol (v/v) at -80 °C.

NMR spectroscopy

NMR data were acquired on a Bruker AVANCE III 600-MHz (14-T) NMR spectrometer with a 5-mm pulsed-field-gradient (*z*-axis) triple HCN probe and were processed using TopSpin v3.2 software. All NMR experiments were conducted at 20 °C, with trimethylsilyl propanoic acid as the ¹H chemical shift reference. Gel-purified RNA in H₂O was centrifuged 10 min at 17,000*g* to sediment any particulate matter. The supernatant RNA was combined with Na₂HPO₄ buffer at pH 7.4 and incubated 1 min at 90 °C then 3 min at ambient temperature. MgCl₂, D₂O, and trimethylsilyl propanoic acid were added to a final volume of 500 µL with 10 mM Na₂HPO₄ (pH 7.4), 2.5 mM MgCl₂, and 90% H₂O/10% D₂O (v/v). The samples were then

incubated 5 min at ambient temperature and stored at 4 °C until data collection. 1D ¹H NMR spectra of the RNA hairpins were collected at 1.12 mM concentration, with 1028 scans. 2D ¹H NOESY spectra in 90% H₂O/10% D₂O (v/v) were acquired with 100 ms mixing time, with 256 scans. A total of 2048 points were taken in F2 and a total of 512 points were taken in F1, with a recycle delay of 1 s and a spectral width of 22 ppm in both dimensions. The RNA concentration was 1.12 mM for the 2D NOESY scans at 20 °C and was 0.47 mM for the 2D NOESY scans at 4 °C. 2D ¹H NOESY spectra of 0.78 mM RNA in 100% D₂O were acquired with 100 ms mixing time, with 256 scans. A total of 2048 points were taken in F2 and a total of 512 points were taken in F1, with a recycle delay of 1 s and a spectral width of 9 ppm in both dimensions.

FRET experiments

FRET spectra were acquired on a HORIBA FluoroLog-3 spectrofluorometer equipped with a Peltier controller and processed using FluorEssence v3.5 software. We combined 1 µM gel-purified RNA in H₂O with Tris (pH 7.5) buffer and incubated it 2 min at 90 °C then 3 min at ambient temperature. KCl and MgCl₂ were added to a final volume of 100 µL with conditions 500 nM RNA, 10 mM Tris (pH 7.5), 100 mM KCl, and 2.5 mM MgCl₂. For experiments with protein binding, HNRNPC was added with the same final buffer conditions. For experiments with denatured RNA, the sample was incubated at least 5 min at 90 °C, and the spectra were measured with the Peltier controller set at 90 °C. The samples were transferred to the cuvette and emission spectra were collected from 500 nm to 750 nm using the excitation wavelength 490 nm, with excitation and emission spectral slit widths of 2 nm and 5 nm, respectively. A buffer solution of 10 mM Tris (pH 7.5), 100 mM KCl, and 2.5 mM MgCl₂ was used as the emission spectrum blank. FRET efficiencies were calculated as $E_{\text{FRET,relative}} = I_{\text{A}} / (I_{\text{D}} + I_{\text{A}})$, where I_{D} is the emission intensity at 518 nm and I_{A} is the emission intensity at 563 nm.

Structural modeling

The 33-nucleotide sequence 5'-UAACUUAU-GUUUUUGCAUUGGACUUUGAGUUA with secondary structure "(((((((((((.....))))))))))", where parentheses denote base pairs and dots denote non-base-paired residues, was used to generate 910 decoy RNA tertiary structures. The decoys varied from one another only in the U0-A32 base pair, where the 5'-most nucleobase U0 was added as a placeholder for the Cy3 fluorophore present in the FRET oligos. Each of the 910 decoys was used to generate 9999 RNA tertiary structure models for the MALAT1 hairpin using the MC-Sym computer program. Within each decoy set, the U0-A32 and A1-U31 base pairs were invariant. The decoy set that generated the most pairs that fit the FRET data for either FI-8-A/m⁶A or FI-26-A/m⁶A was used to select models for the methylated and unmethylated hairpins. Rather than assigning weights to the various experimental parameters, we used the experimental data as filters in a sequential fashion, and the final selected models do not depend on the order of application of the filters.

Models were selected from the 9999 structural models in the decoy set based on four simultaneous criteria: (1) best fit to the FRET data, (2) best fit to the 2D NOESY data, (3) best P-Scores, and (4) maximization of relative FRET yields.

- (1) Best fit to the FRET data: the theoretical FRET efficiencies were calculated as

$$E_{\text{FRET,relative}} = \frac{1}{1 + (R^6/R_0^6)}$$

with

$$R_0^6 = (55.7 \text{ \AA})^6 \cdot K^2 \cdot 3/2$$

and

$$K = \mathbf{D} \cdot \mathbf{A} - 3(\mathbf{R} \cdot \mathbf{D})(\mathbf{R} \cdot \mathbf{A})$$

where \mathbf{D} and \mathbf{A} are the unit vectors oriented from N1 to C4 of the uridine nucleotides corresponding to the donor and acceptor fluorophores, respectively; \mathbf{R} is the unit vector oriented from the donor position H3 to the acceptor position H3; and R is the distance from the donor H3 to the acceptor H3. Only pairs of structures for which the theoretical $E_{\text{FRET}}(\text{A})/E_{\text{FRET}}(\text{m}^6\text{A})$ ratios were within 0.01 of the experimental ratios for FI-8-A/m⁶A and FI-26-A/m⁶A were kept (122,844 A/m⁶A pairs).

- (2) Best fit to the 2D NOESY data: to extract inter-proton distance information from the 2D NOESY data at 20 °C in 10% D₂O with 100 ms mixing time, we assumed a linear relationship between peak intensity and mixing time:

$$\eta = 2W_0 t_{\text{mix}}$$

where η is the NOE peak intensity, W_0 is the rate of the zero-quantum transition, and t_{mix} is the mixing time (100 ms). With the use of this approximation, the inter-proton distance r is related to the peak intensity by

$$r^6 \propto \frac{1}{W_0} \propto \frac{1}{\eta};$$

thus, the experimental NOE intensities and the relative distances between imino protons in the modeled tertiary structures were used to calculate $\log(r_x^6/r_0^6)$ ratios, where r_x is the inter-proton distance for a pair of imino protons and r_0 is the distance between G27 H1 and U5 H3. The least-squares differences between the five experimental and modeled $\log(r_x^6/r_0^6)$ ratios were then used to classify the modeled structures as either A or m⁶A depending on whether they were a closer fit to the unmethylated or methylated hairpin, respectively. Using this method, we assigned 8176 structures as A, while we assigned 1823 as m⁶A. Only pairs of structures for which the A and m⁶A assignments were consistent with the assignments based on the FRET efficiencies were kept.

- (3) Best P-Scores: the P-Score for each modeled RNA tertiary structure was calculated based on the

phosphate chain torsion angles in the predicted tertiary structures as described previously [39]. P-Scores involve as many as four consecutive phosphate groups, and their aim is to assess how natural the modeled RNA looks like given the backbone trace. Only the top 5000 of the 9999 tertiary structures in the decoy set were kept.

- (4) Maximization of relative FRET yields: once the original 9999 structures in the decoy set were filtered based on their FRET fit, NOE fit, and P-Scores, there were 276 remaining structures corresponding to the unmethylated hairpin, and 713 structures corresponding to the methylated hairpin. These were narrowed down to 25 models each corresponding to the unmethylated and methylated hairpins by maximizing the density of A/m⁶A pairs. A structural model that has been selected to be a representative of the A state (Fig. 6a, gray dots) must maximize the number of structural models in the m⁶A state (Fig. 6a, dark red dots) for which the relative FRET efficiency yielded is close to the one experimentally observed (gray lines connecting the dots) in order to achieve density maximization. The same principle was applied while populating the m⁶A state; models must maximize the number of A state relative FRET yields.

Acknowledgments

This work was supported by the National Institutes of Health (DP1GM105386 and R01GM113194 to T.P.; K01HG006699 to Q.D.) and the National Institutes of Health Medical Scientist Training Program Grant NIGMS T32GM007281 (K.I.Z.). The authors would like to thank the generous support of the University of Chicago Biological Sciences Division and the Frank Family Endowment (K.I.Z.).

Received 22 July 2015;

Received in revised form 25 August 2015;

Accepted 27 August 2015

Available online 4 September 2015

Keywords:

N⁶-methyladenosine (m⁶A);
MALAT1 lncRNA;
FRET;
NMR;
RNA structural modeling

Abbreviations used:

MALAT1, metastasis associated lung adenocarcinoma transcript 1; HNRNPC, heterogeneous nuclear ribonucleoprotein C; FRET, Förster resonance energy transfer; NOESY, nuclear Overhauser enhancement spectroscopy; NOE, nuclear Overhauser enhancement.

References

- [1] T.M. Carlile, M.F. Rojas-Duran, B. Zinshteyn, H. Shin, K.M. Bartoli, W.V. Gilbert, Pseudouridine profiling reveals regulated mRNA pseudouridylation in yeast and human cells, *Nature* 515 (2014) 143–146, <http://dx.doi.org/10.1038/nature13802>.
- [2] R. Desrosiers, K. Friderici, F. Rottman, Identification of methylated nucleosides in messenger RNA from Novikoff hepatoma cells, *Proc. Natl. Acad. Sci.* 71 (1974) 3971–3975.
- [3] D. Dominissini, S. Moshitch-Moshkovitz, S. Schwartz, M. Salmon-Divon, L. Ungar, S. Osenberg, et al., Topology of the human and mouse m⁶A RNA methylomes revealed by m⁶A-seq, *Nature* 485 (2012) 201–206, <http://dx.doi.org/10.1038/nature11112>.
- [4] K.D. Meyer, Y. Saletore, P. Zumbo, O. Elemento, C.E. Mason, S.R. Jaffrey, Comprehensive analysis of mRNA methylation reveals enrichment in 3' UTRs and near stop codons, *Cell* 149 (2012) 1635–1646, <http://dx.doi.org/10.1016/j.cell.2012.05.003>.
- [5] J.E. Squires, H.R. Patel, M. Nusch, T. Sibbritt, D.T. Humphreys, B.J. Parker, et al., Widespread occurrence of 5-methylcytosine in human coding and non-coding RNA, *Nucleic Acids Res.* 40 (2012) 5023–5033, <http://dx.doi.org/10.1093/nar/gks144>.
- [6] S. Schwartz, S.D. Agarwala, M.R. Mumbach, M. Jovanovic, P. Mertins, A. Shishkin, et al., High-resolution mapping reveals a conserved, widespread, dynamic mRNA methylation program in yeast meiosis, *Cell* 155 (2013) 1409–1421, <http://dx.doi.org/10.1016/j.cell.2013.10.047>.
- [7] T. Pan, N⁶-Methyl-adenosine modification in messenger and long non-coding RNA, *Trends Biochem. Sci.* 38 (2013) 204–209, <http://dx.doi.org/10.1016/j.tibs.2012.12.006>.
- [8] J. Liu, Y. Yue, D. Han, X. Wang, Y. Fu, L. Zhang, et al., A METTL3–METTL14 complex mediates mammalian nuclear RNA N⁶-adenosine methylation, *Nat. Chem. Biol.* 10 (2013) 93–95, <http://dx.doi.org/10.1038/nchembio.1432>.
- [9] X.-L. Ping, B.-F. Sun, L. Wang, W. Xiao, X. Yang, W.-J. Wang, et al., Mammalian WTAP is a regulatory subunit of the RNA N⁶-methyladenosine methyltransferase, *Cell Res.* 24 (2014) 177–189, <http://dx.doi.org/10.1038/cr.2014.3>.
- [10] G. Zheng, J.A. Dahl, Y. Niu, P. Fedorcsak, C.-M. Huang, C.J. Li, et al., ALKBH5 is a mammalian RNA demethylase that impacts RNA metabolism and mouse fertility, *Mol. Cell* (2012) <http://dx.doi.org/10.1016/j.molcel.2012.10.015>.
- [11] G. Jia, Y. Fu, X. Zhao, Q. Dai, G. Zheng, Y. Yang, et al., N⁶-Methyladenosine in nuclear RNA is a major substrate of the obesity-associated FTO, *Nat. Chem. Biol.* 7 (2011) 885–887, <http://dx.doi.org/10.1038/nchembio.687>.
- [12] J.-M. Fustin, M. Doi, Y. Yamaguchi, H. Hida, S. Nishimura, M. Yoshida, et al., RNA-methylation-dependent RNA processing controls the speed of the circadian clock, *Cell* 155 (2013) 793–806, <http://dx.doi.org/10.1016/j.cell.2013.10.026>.
- [13] S. Geula, S. Moshitch-Moshkovitz, D. Dominissini, A.A. Mansour, N. Kol, M. Salmon-Divon, et al., Stem cells. m⁶A mRNA methylation facilitates resolution of naïve pluripotency toward differentiation, *Science* 347 (2015) 1002–1006, <http://dx.doi.org/10.1126/science.1261417>.
- [14] P.J. Batista, B. Molinie, J. Wang, K. Qu, J. Zhang, L. Li, et al., m⁶A RNA modification controls cell fate transition in mammalian embryonic stem cells, *Cell Stem Cell* 15 (2014) 707–719, <http://dx.doi.org/10.1016/j.stem.2014.09.019>.
- [15] Y. Wang, Y. Li, J.I. Toth, M.D. Petroski, Z. Zhang, J.C. Zhao, N⁶-Methyladenosine modification destabilizes developmental regulators in embryonic stem cells, *Nat. Cell Biol.* 16 (2014) 191–198, <http://dx.doi.org/10.1038/ncb2902>.
- [16] Y. Niu, X. Zhao, Y.-S. Wu, M.-M. Li, X.-J. Wang, Y.-G. Yang, N⁶-Methyl-adenosine (m⁶A) in RNA: An old modification with a novel epigenetic function, *Genomics, Proteomics Bioinf.* 11 (2013) 8–17, <http://dx.doi.org/10.1016/j.gpb.2012.12.002>.
- [17] Y. Fu, D. Dominissini, G. Rechavi, C. He, Gene expression regulation mediated through reversible m⁶A RNA methylation, *Nat. Rev. Genet.* 15 (2014) 293–306, <http://dx.doi.org/10.1038/nrg3724>.
- [18] X. Wang, Z. Lu, A. Gomez, G.C. Hon, Y. Yue, D. Han, et al., N⁶-Methyladenosine-dependent regulation of messenger RNA stability, *Nature* 505 (2014) 117–120, <http://dx.doi.org/10.1038/nature12730>.
- [19] N. Liu, Q. Dai, G. Zheng, C. He, M. Parisien, T. Pan, N⁶-Methyladenosine-dependent RNA structural switches regulate RNA–protein interactions, *Nature* 518 (2015) 560–564, <http://dx.doi.org/10.1038/nature14234>.
- [20] D. Theler, C. Dominguez, M. Blatter, J. Boudet, F.H.-T. Allain, Solution structure of the YTH domain in complex with N⁶-methyladenosine RNA: A reader of methylated RNA, *Nucleic Acids Res.* 42 (2014) 13911–13919, <http://dx.doi.org/10.1093/nar/gku1116>.
- [21] C. Xu, X. Wang, K. Liu, I.A. Roundtree, W. Tempel, Y. Li, et al., Structural basis for selective binding of m⁶A RNA by the YTHDC1 YTH domain, *Nat. Chem. Biol.* 10 (2014) 927–929, <http://dx.doi.org/10.1038/nchembio.1654>.
- [22] S. Luo, L. Tong, Molecular basis for the recognition of methylated adenines in RNA by the eukaryotic YTH domain, *Proc. Natl. Acad. Sci.* 111 (2014) 13834–13839, <http://dx.doi.org/10.1073/pnas.1412742111>.
- [23] C. Roost, S.R. Lynch, P.J. Batista, K. Qu, H.Y. Chang, E.T. Kool, Structure and thermodynamics of N⁶-methyladenosine in RNA: A spring-loaded base modification, *J. Am. Chem. Soc.* 137 (2015) 2107–2115, <http://dx.doi.org/10.1021/ja513080v>.
- [24] E. Kierzek, The thermodynamic stability of RNA duplexes and hairpins containing N⁶-alkyladenosines and 2-methylthio-N⁶-alkyladenosines, *Nucleic Acids Res.* 31 (2003) 4472–4480, <http://dx.doi.org/10.1093/nar/gkg633>.
- [25] K. Zarnack, J. König, M. Tajnik, I. Martincorena, S. Eustermann, I. Stévant, et al., Direct competition between hnRNP C and U2AF65 protects the transcriptome from the exonization of Alu elements, *Cell* 152 (2013) 453–466, <http://dx.doi.org/10.1016/j.cell.2012.12.023>.
- [26] Z. Cieniková, F.F. Damberger, J. Hall, F.H.-T. Allain, C. Maris, Structural and mechanistic insights into poly(uridine) tract recognition by the hnRNP C RNA recognition motif, *J. Am. Chem. Soc.* 136 (2014) 14536–14544, <http://dx.doi.org/10.1021/ja507690d>.
- [27] Y. Wan, M. Kertesz, R.C. Spitale, E. Segal, H.Y. Chang, Understanding the transcriptome through RNA structure, *Nat. Rev. Genet.* 12 (2011) 641–655, <http://dx.doi.org/10.1038/nrg3049>.
- [28] R.C. Spitale, R.A. Flynn, Q.C. Zhang, P. Crisalli, B. Lee, J.-W. Jung, et al., Structural imprints *in vivo* decode RNA regulatory mechanisms, *Nature* 519 (2015) 486–490, <http://dx.doi.org/10.1038/nature14263>.
- [29] N. Liu, M. Parisien, Q. Dai, G. Zheng, C. He, T. Pan, Probing N⁶-methyladenosine RNA modification status at single nucleotide resolution in mRNA and long noncoding RNA, *RNA* 19 (2013) 1848–1856, <http://dx.doi.org/10.1261/rna.041178.113>.
- [30] K. Darty, A. Denise, Y. Ponty, VARNA: Interactive drawing and editing of the RNA secondary structure, *Bioinformatics*

- 25 (2009) 1974–1975, <http://dx.doi.org/10.1093/bioinformatics/btp250>.
- [31] M. Parisien, F. Major, The MC-Fold and MC-Sym pipeline infers RNA structure from sequence data, *Nature* 452 (2008) 51–55, <http://dx.doi.org/10.1038/nature06684>.
- [32] M.P. Latham, D.J. Brown, S.A. McCallum, A. Pardi, NMR methods for studying the structure and dynamics of RNA, *ChemBioChem* 6 (2005) 1492–1505, <http://dx.doi.org/10.1002/cbic.200500123>.
- [33] L. Zidek, R. Stefl, V. Sklenár, NMR methodology for the study of nucleic acids, *Curr. Opin. Struct. Biol.* 11 (2001) 275–281.
- [34] S. Weiss, Measuring conformational dynamics of biomolecules by single molecule fluorescence spectroscopy, *Nat. Struct. Mol. Biol.* 7 (2000) 724–729, <http://dx.doi.org/10.1038/78941>.
- [35] E.A. Alemán, R. Lamichhane, D. Rueda, Exploring RNA folding one molecule at a time, *Curr. Opin. Chem. Biol.* 12 (2008) 647–654, <http://dx.doi.org/10.1016/j.cbpa.2008.09.010>.
- [36] C.R. Alarcón, H. Lee, H. Goodarzi, N. Halberg, S.F. Tavazoie, N⁶-Methyladenosine marks primary microRNAs for processing, *Nature* 519 (2015) 482–485, <http://dx.doi.org/10.1038/nature14281>.
- [37] C.R. Alarcón, H. Goodarzi, H. Lee, X. Liu, S. Tavazoie, S.F. Tavazoie, HNRNPA2B1 is a mediator of m⁶A-dependent nuclear RNA processing events, *Cell* 162 (2015) 1299–1308, <http://dx.doi.org/10.1016/j.cell.2015.08.011>.
- [38] Q. Dai, R. Fong, M. Saikia, D. Stephenson, Y.-t. Yu, T. Pan, et al., Identification of recognition residues for ligation-based detection and quantitation of pseudouridine and N⁶-methyladenosine, *Nucleic Acids Res.* 35 (2007) 6322–6329, <http://dx.doi.org/10.1093/nar/gkm657>.
- [39] M. Parisien, J.A. Cruz, E. Westhof, F. Major, New metrics for comparing and assessing discrepancies between RNA 3D structures and models, *RNA* 15 (2009) 1875–1885, <http://dx.doi.org/10.1261/ma.1700409>.